Available online at www.sciencedirect.com
ScienceDirect
Trans. Nonferrous Met. Soc. China 34(2024) 4005−4019
Transactions of Nonferrous Metals Society of China
www.tnmsc.cn

Enhanced mechanical and electrical properties of multi-walled carbon nanotubes reinforced Cu/Ti_3SiC_2/C nanocomposites via high-pressure torsion

Zi-xuan WU[1,2,3], Pei-fan ZHANG[4], Xiao-song JIANG[1,2], Hong-liang SUN[1,2], Yan-jun LI[5], Pål CHRISTIAN[5], Liu YANG[6]

1. Key Laboratory of Advanced Technologies of Materials, Ministry of Education, Southwest Jiaotong University, Chengdu 610031, China;
2. School of Materials Science and Engineering, Southwest Jiaotong University, Chengdu 610031, China;
3. School of Engineering and Materials Science, Queen Mary University of London, London E1 4NS, United Kingdom;
4. Teaching and Research Support Center, Naval Aviation University, Yantai 264001, China;
5. Department of Materials Science and Engineering, Norwegian University of Science and Technology, Trondheim 7491, Norway;
6. Institute for Applied Materials, Karlsruhe Institute of Technology, Karlsruhe 76131, Germany

Received 30 April 2023; accepted 21 September 2023

Abstract: In order to achieve combined mechanical and electrical properties, multi-walled carbon nanotubes (MWCNTs) reinforced Cu/Ti_3SiC_2/C nanocomposites were further processed by high-pressure torsion (HPT). The maximum microhardness values of central and edge from the composites with 1 wt.% MWCNTs reached HV 130.0 and HV 363.5, which were 43.9% and 39.5% higher than those of the original samples, respectively. With the same content of MWCNTs, its electrical conductivity achieved 3.42×10^7 S/m, which was increased by 78.1% compared with that of original samples. The synergistic improvement of mechanical and electrical properties is attributed to the obtained microstructure with increased homogenization and refinement, as well as improved interfacial bonding and reduced porosity. The strengthening mechanisms include dispersion and refinement strengthening for mechanical properties, as well as reduced electron scattering for electrical properties.

Key words: Cu/Ti_3SiC_2/C nanocomposites; multi-walled carbon nanotubes; high-pressure torsion; microstructure; microhardness; electrical conductivity

1 Introduction

The development of Cu/Ti_3SiC_2/C composites is based on Cu/graphite composites, which are widely used in areas including electrical contact and friction, with combined mechanical and electrical properties [1,2]. In Cu/Ti_3SiC_2/C composites, graphite can be used as lubricating phase to reduce friction, while Ti_3SiC_2 has high strength and a coefficient of thermal expansion close to that of Cu matrix, which can be used as reinforcing phase to improve mechanical properties and interfacial bonding [3−6]. In order to further improve the mechanical and electrical properties of the composites, as well as utilizing the concept of hybrid reinforcement, we proposed to use multi-walled carbon nanotubes (MWCNTs) as another

Corresponding author: Xiao-song JIANG, Tel: +86-28-87634177, E-mail: xsjiang@swjtu.edu.cn;
Yan-jun LI, Tel: +47-73551206, E-mail: yanjun.li@ntnu.no
DOI: 10.1016/S1003-6326(24)66654-9

reinforcing phase [1,7−10]. The reason is that the unique hollow tubular structure of MWCNTs gives them not only the inherent mechanical properties of carbon materials (elastic modulus of 1.2 TPa and strength of 100 GPa), but also metal-like electrical and thermal conductivities (electrical conductivity of 10^6−10^7 S/m and thermal conductivity of 6000 W/(m·K) [11,12]. In addition, MWCNTs are easier to prepare and have better mechanical properties than carbon nanotubes (CNTs) [13]. However, due to their nano-scale size, as well as large specific surface area and aspect ratio, MWCNTs are highly susceptible to agglomeration and difficult to achieve well-dispersion in Cu matrix, which seriously affects their applications [14]. In addition, the interfacial wettability between MWCNTs and Cu matrix is poor, and the interfaces are incompatible or even completely separated [14]. Therefore, it is of great importance to effectively disperse MWCNTs to obtain the homogenized microstructure, as well as improve the interfacial bonding in the composites.

A proper preparation method is important to obtain the homogenized microstructure and favorable comprehensive properties [15,16]. Powder metallurgy based on solid-state route is widely used in fabricating copper matrix composites since ball milling enables the homogeneous mixing of all components [2,17−20]. However, in practice, the contribution of ball milling to the dispersion of MWCNTs is quite limited since ball milling may lead to structural changes of MWCNTs due to the induced energy and elevated temperature [8]. Recent researches have suggested that cryogenic milling can partially mitigate the adverse effects of high-temperature densification process [21,22]. Therefore, surface modification and further processing that can address the issues above are necessary [1,13,23−28]. Firstly, the surface modification can improve the dispersibility of MWCNTs by functionalizing their surfaces through chemical processes [14,29−35]. In this work, gallic acid solution was chosen to modify the surface of MWCNTs, by grafting hydrophilic functional groups to overcome their hydrophobic nature and agglomeration [3−6]. Secondly, a series of physical processes based on severe plastic deformation (SPD) can further introduce energy to significantly reduce or eliminate the agglomeration of MWCNTs [9,19,21,36,37], including equal-channel angular pressing (ECAP) [38], accumulative roll-bonding (ARB) [39,40], friction stir processing (FSP) [41], and high-pressure torsion (HPT). Similarly, in this work, HPT was selected for further treatment to effectively achieve the homogenization and refinement of the microstructure [11,12,42,43]. On the one hand, HPT is a physical process, which does not involve chemical reactions and can preserve all phases in the composites. On the other hand, HPT is able to break grains and eliminate pores while dispersing MWCNTs by simultaneously applying extreme pressure and shear strain [6]. As a result, HPT can improve mechanical properties based on dispersion and refinement strengthening, and enhance electrical properties due to improved interfacial bonding and reduced porosity [8].

Based on our previous work [3], the effect of MWCNTs content on the comprehensive properties of the composites before HPT was analyzed, and the optimal content of MWCNTs was selected for subsequent microstructure characterization. In order to further improve the mechanical and electrical properties of Cu/Ti_3SiC_2/C/MWCNTs composites, HPT was performed based on powder metallurgy, aiming at obtaining the microstructure with significantly increased homogenization and refinement, as well as improved interfacial bonding between MWCNTs and Cu matrix. The effects of HPT treatment and HPT turns on the microstructure and properties of the composites were investigated. Then, the strengthening mechanisms of HPT-treated composites were summarized.

2 Experimental

2.1 Raw materials and fabrication of sample

Cu/Ti_3SiC_2/C/MWCNTs composites with different MWCNTs contents were prepared according to the preparation procedure in our previous work [3]. Some properties of raw materials used in the experiment are shown in Table 1, including Cu (Chengdu Huayin Powder Technology Company Ltd.), Ti_3SiC_2 (Forsman Scientific (Beijing) Company Ltd.), C (Cixi Xincheng Sealing Material Company Ltd.), and MWCNTs (Chengdu Organic Chemicals Company Ltd., Chinese Academy of Sciences). Three groups of composites with different MWCNTs contents were prepared using the raw materials above, where the mass fractions of each component were Ti_3SiC_2

Table 1 Some properties of raw materials

Raw material	Density/ ($g \cdot cm^{-3}$)	Size	Purity/%
Cu	8.89	≤60 μm	≥99.99
Ti_3SiC_2	4.53	≤50 μm	≥99
C	2.2	≤75 μm	≥99.9
MWCNTs	2.1	Diameter: 20−30 nm; Length: 10−30 μm	≥95

(10%), C (3%), and MWCNTs (1%, 5%, and 9%), respectively. The MWCNTs were firstly surface modified and dispersed in 10 μg/mL gallic acid solution. Cu/Ti_3SiC_2/C/MWCNTs composites were obtained after the sequence of ball milling, freeze drying, hot pressing, and sintering.

The composites were further subjected to HPT in order to alleviate the side effects of MWCNTs agglomeration while achieving grain refinement, and improving mechanical and electrical properties [6]. Based on MTS 311 material testing system with a maximum force of 2 MN and a maximum torque of 1.5 N·m at Norwegian University of Science and Technology (NTNU), the HPT process was performed in experiment after modifications. Four groups of samples with different HPT turns were prepared at a pressure of 6 GPa (0, 0.5, 2, and 5 turns, respectively). The fabrication process of the composites is shown in Fig. 1.

2.2 Characterization

The relative density of the composites was tested based on Archimedes principle. The mechanical properties were obtained from Vickers hardness tester (HV, HXD−100TM) with a load force of 1 kg and a dwell time of 15 s. The electrical properties were measured by using a resistivity tester (Sigmatest 2.069). The characterization of microstructure involved X-ray diffraction (XRD, Rigaku Ultma IV) with 2θ between 10° and 80°, optical microscope (OM, AxioCam MRc5), scanning electron microscope (SEM, JEM−100CX) with back-scattered electron (BSE) imaging mode and energy dispersive X-ray spectrometer (EDS), electron back-scattered diffractometer (EBSD, Oxford NordlysMax3), and transmission electron microscope (TEM, FEI Tecnai F20ST with 200 kV accelerating voltage).

3 Results and discussion

3.1 Mechanical and electrical properties

Table 2 shows the mechanical and electrical properties of raw samples with different MWCNTs contents before HPT [3]. We found that as MWCNTs content increased, the relative density gradually decreased, and the mechanical properties first increased and then decreased, in contrast to the changes in the electrical properties. The reasons for the emergence of different trends was discussed in

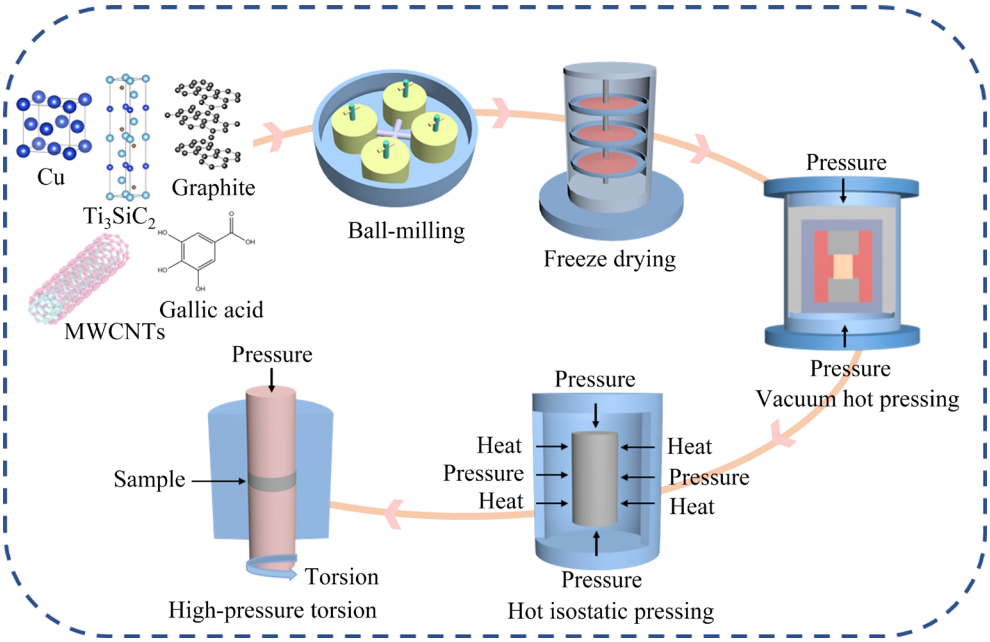

Fig. 1 Schematic diagram of fabricating Cu/Ti_3SiC_2/C/MWCNTs nanocomposites

Table 2 Relative density, mechanical, and electrical properties of Cu/Ti_3SiC_2/C/MWCNTs composites with different MWCNTs contents [3]

MWCNTs content/ wt.%	Relative density/%	Microhardness (HV)	Electrical conductivity/ (10^7 S·m^{-1})
1	93.51	64.9	1.92
5	87.91	68.5	1.18
9	82.84	45.5	2.32

our previous work [3,44,45]. Since the target of this work is to obtain the composites with combined mechanical and electrical properties, we suggested that the composites containing 1 wt.% MWCNTs had the best overall performance, and we mainly selected samples with this composition in subsequent microstructure characterization.

The mechanical and electrical properties of the composites will change significantly after HPT. Figure 2 shows the relationship between relative density and HPT turns. The relative density of the composites gradually increases with the increase of HPT turns, but the tendency of the increment tends to level off. This is because with increasing HPT turns, that is, the improvement of applied pressure and shear strain, the plastic deformation of the microstructure will make internal pores to be closed substantially [12]. At the same time, the energy introduced inwards generates plenty of non-equilibrium high-angle grain boundaries (HAGBs), which promotes the interactions between grain boundaries and dislocations, thus improving the densification of microstructure while refining grains [30]. However, the effect of mechanical densification is limited. As HPT turns continuously increase, the plastic deformation of the microstructure also gradually approaches the maximum, and the pores tend to be saturated. Therefore, the trend of improving relative density leveled off by further increasing HPT turns. In addition, comparing the relative density of the composites with different MWCNTs contents, it was found that HPT was more effective in improving the relative density when the raw sample owned a lower value.

The mechanical properties of the composites after HPT were fully analyzed. To begin with, it should be noted that it is not the case that the higher the MWCNTs content, the higher the microhardness of the composites. Combined with Table 2, the microhardness of the composites first increases and then decreases as the content of MWCNTs increases. The first increase is due to the high strength and microhardness of MWCNTs, and their incorporation greatly increases the number and area of interfaces in the composites, further improves mechanical properties by grain refinement [13,25,45]. However, when MWCNTs content reaches 9 wt.%, the poor dispersion and wettability of MWCNTs with Cu matrix cause more serious agglomeration, resulting in the inhomogeneity between different regions and the decrease in microhardness.

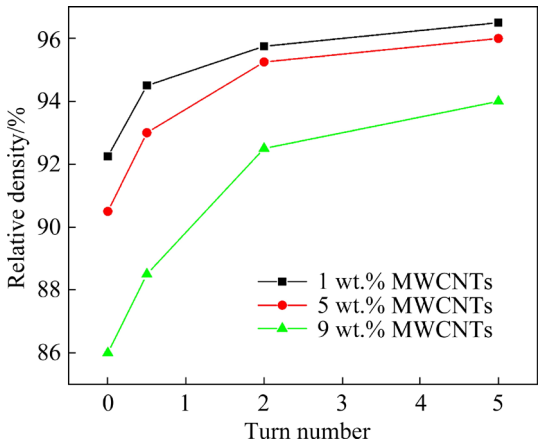

Fig. 2 Relative density of Cu/Ti_3SiC_2/C/MWCNTs nanocomposites with different MWCNTs contents and HPT turns

After different HPT turns, the relative density of the composites was enhanced, so did the microhardness. Figure 3 shows three-dimensional (3D) microhardness distribution of the composites with 1 wt.% MWCNTs (33 microhardness values at fixed positions were selected for each group of samples, and a coordinate system was constructed on sample surface, with sample center as origin and the microhardness value as *Z*-axis, to make a 3D microhardness distribution of the composites, while the magnitude of the microhardness was mapped on a two-dimensional (2D) plane). As shown in Fig. 3, the microhardness of the composites changes in a gradient with increasing distance from sample center. When HPT turn N=0.5, the microhardness of sample center and edge are HV 90.5 and HV 260.5, with an increment of HV 170. The microhardness distributions satisfy similar patterns at HPT turns of N=2 and N=5. Compared with raw samples without HPT, the microhardness values after HPT were

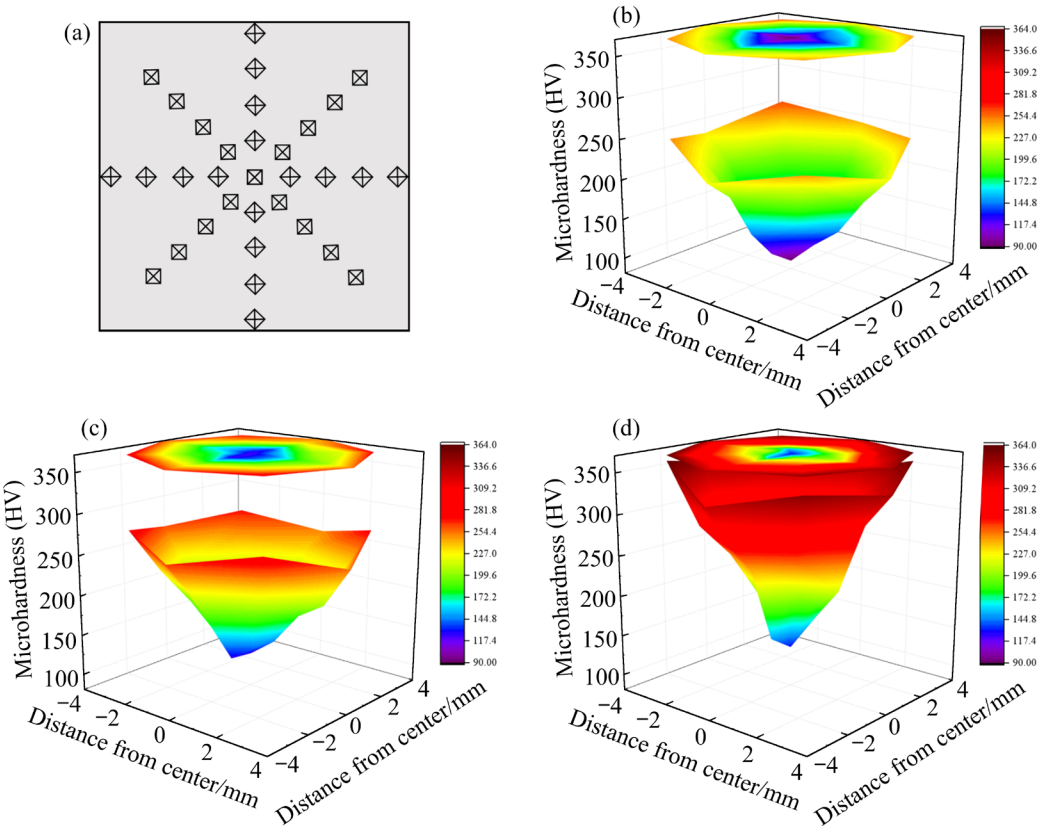

Fig. 3 3D microhardness distribution of Cu/Ti_3SiC_2/C/MWCNTs nanocomposites with 1 wt.% MWCNTs at different HPT turns (N): (a) Schematic diagram of microhardness test; (b) N=0.5; (c) N=2; (d) N=5

significantly improved with the increase of HPT turns. As the number of HPT turns N increased from 0.5 to 5, the microhardness of the sample center was gradually enhanced from HV 90.5 to HV 130.0, and that of the edge was improved from HV 260.5 to HV 363.5, which was increased by 43.9% and 39.5%, respectively. The microhardness distributions of different samples after HPT are similar, and all of them have less microhardness in central region and more microhardness in edge. Besides, during the transition from the central to the edge, there are obvious stages in the microhardness of local areas near the edge. This is because the shear strain introduced by HPT gradually increases from the central to the edge of the samples, resulting in the formation of a gradient microstructure in the composites [9,11,26,36].

Cu/C composites usually require excellent electrical properties, so it is necessary to investigate their electrical conductivity. Combined with Table 2, the composites with 9 wt.% MWCNTs had the highest electrical conductivity, reaching 2.32×10^7 S/m for raw samples, while the composites with 5 wt.% MWCNTs had the lowest one. The electrical conductivity decreased with the increase of MWCNTs content during initial stage. The reasons are, on the one hand, the problem of interfacial bonding between MWCNTs and Cu matrix. With the increase of MWCNTs content, the phenomenon of MWCNTs agglomeration will become more obvious, resulting in a certain extent of pores inevitably. On the other hand, the wettability between MWCNTs and Cu matrix is poor, almost no chemical reaction occurs, and the interfacial bonding between the two phases always relies on thermal diffusion between atoms during fabrication, thus the interfacial bonding mainly defined as mechanical bonding [13,14,45]. However, when MWCNTs content is high enough, they can be interconnected with each other to form a continuous 3D net structure. That is, electron conduction channels are formed, leading to the elevated electrical conductivity.

Figure 4 shows the relationship between electrical conductivity and HPT turns. The electrical conductivity of the composites was improved with increasing HPT turns, and the trend was very similar to that of relative density. The electrical

conductivity of the composites containing 1 wt.% MWCNTs reached 3.42×10^7 S/m after HPT (N=5), which was 78.1% higher compared to that before HPT. Combined with previous analysis of relative density, the samples with different MWCNTs contents all produced grain refinement and gradual decrease in porosity with increasing HPT turns. Due to the densification of the composites and improvement of interfacial bonding, the scattering of carriers by defects such as dislocations near phase interfaces and pores is weakened, thus achieving the enhanced electrical conductivity [12,26].

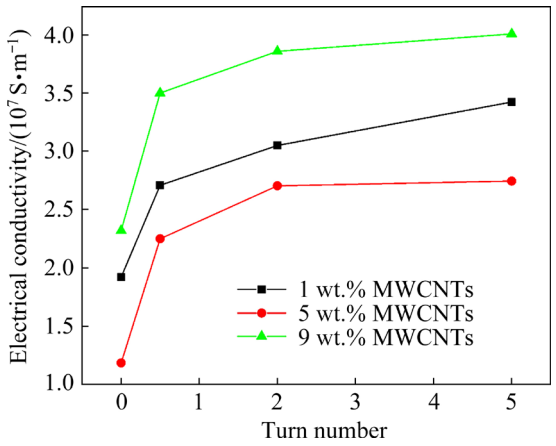

Fig. 4 Electrical conductivity of Cu/Ti_3SiC_2/C/MWCNTs nanocomposites with different MWCNTs contents and HPT turns

In short, the relative density, microhardness, and electrical conductivity of Cu/Ti_3SiC_2/C/MWCNTs nanocomposites were significantly improved after HPT. Since the samples are subjected to shear strain proportional to the distance from the center, the plastic deformation occurring at different locations of the samples differs from the center to edge. Therefore, the properties of the composites after HPT also showed a gradient from the center to edge.

3.2 Microstructure

Since the composites with 1 wt.% MWCNTs have the best overall performance, we mainly chose the samples with this composition for the microstructure characterization. Figure 5 shows XRD patterns of the composites. It is widely accepted that HPT is a purely physical process, with large plastic deformation and no chemical reactions occurring [6]. Therefore, the phase composition of the composites did not change after HPT. With increasing HPT turns, the microstructure of the composites will change significantly, though the phase composition remains unchanged. On the one hand, the diffraction peaks of Cu matrix in the composites are higher than those of raw samples. This is due to the slight differences from texture structure caused by HPT, which makes the peak intensity increase. On the other hand, the width of diffraction peaks increases with increasing HPT turns. This is caused by grain refinement and lattice distortion in Cu matrix. In addition, the appearance of new phases including TiC and Cu_9Si is due to the thermal decomposition of Ti_3SiC_2 at high temperatures [3−6]. We also found that the C(002) peak was relatively obvious when HPT turn N=0.5 [6].

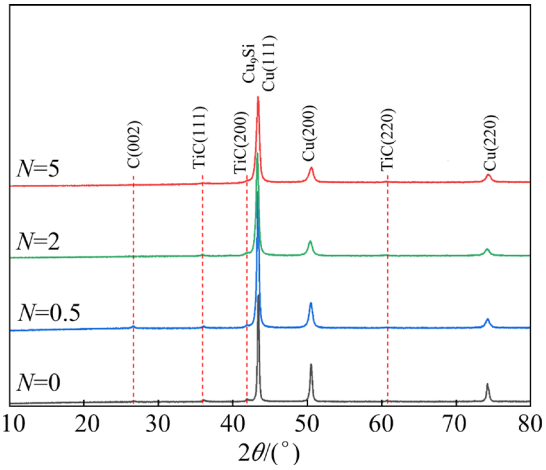

Fig. 5 XRD patterns of Cu/Ti_3SiC_2/C/MWCNTs nanocomposites with 1 wt.% MWCNTs at different HPT turns

Figure 6 shows metallographic morphologies of the composites. When HPT turn N=0.5, there is certain independence between different phases in the composites. There is a clear distinction between the black carbon-containing phases and white Cu matrix, and the presence of some pores was also observed. With increasing HPT turns, the blending of different phases rises significantly, the interfaces become less obvious, and the number of pores gradually decreases. At the same time, the particle size of each phase reduces with increasing HPT turns, thus significant grain refinement can be observed. When HPT turn reaches N=5, it can be seen that the most obvious directionality has been left in microstructure after HPT, and the grain size reaches the minimum.

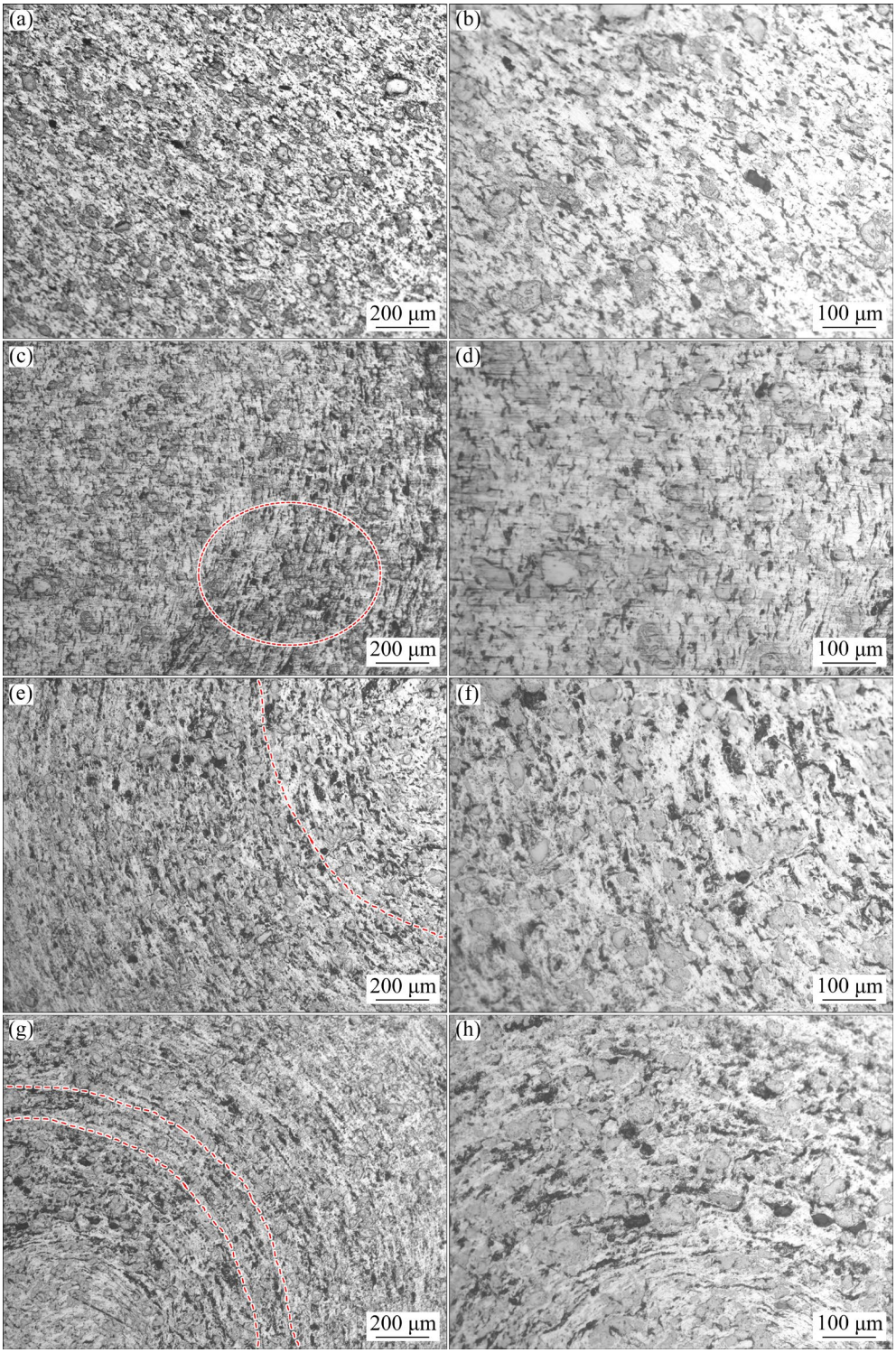

Fig. 6 Optical images of Cu/Ti_3SiC_2/C/MWCNTs nanocomposites with 1 wt.% MWCNTs at different HPT turns: (a, b) N=0; (c, d) N=0.5; (e, f) N=2; (g, h) N=5

According to HPT theory, the farther distance from the center of the samples subjected to a higher torque is, the greater the plastic deformation is. As shown in Figs. 6(g, h), due to shear strain provided by the HPT, the grains undergo shear deformation, and both reinforcing phases and matrix are significantly elongated with band morphology. With the increase of HPT turns, the plastic deformation intensifies, and the accumulation of deformation leads to the disorder of grain morphology, thus the grains are obviously elongated. To some extent, the blending between

MWCNTs and Cu matrix was effectively improved, and the dispersion inhomogeneity of MWCNTs due to their own agglomeration was solved [26]. At the same time, increasing HPT turns also makes the grain size of Cu matrix refiner, which significantly improves refinement strengthening [8].

In order to further investigate the distribution of reinforcing phases in the composites after HPT, as well as the evolution of the microstructure during HPT, the composites containing 1 wt.% MWCNTs at different HPT turns were further characterized by SEM. As shown in Fig. 7, the number of C atoms at Position 1 accounts for 87.17%, which tentatively proves that the black region is mainly composed of carbon-containing phases. Point 2 was taken at the interfaces between carbon-containing phases and Cu matrix, and various elements were distributed. Point 3 was sampled in gray region and judged to be Ti_3SiC_2. The low content of Si element is due to the tendency of thermal decomposition of Ti_3SiC_2 at high temperatures [3−6]. The number of obvious phase interfaces decreases after HPT, and the interfaces tend to blur. The color difference between different phases is reduced, and localized reinforcing phases clustering is hardly visible. The homogeneous distribution of reinforcing phases in Cu matrix is demonstrated, as well as the improvement of the microstructure homogeneity of the composites by HPT [1,8].

Figure 8 shows EBSD results of the composites. Figure 8(a) shows the degree of local mismatch within the microstructure. The overall relatively low degree of local mismatch indicates that the strain within the composites is uniform and low, demonstrating that the distribution homogeneity of reinforcing phases in Cu matrix has been significantly improved after HPT [7]. It is possible that differences in phase composition cause color differences between different regions, and the regions with a higher degree of local mismatch may contain interfaces and reinforcing phases. In addition, the contours of grain boundaries are not obvious, indicating that most of them are low-angle grain boundaries (LAGBs) [12]. Figure 8(b) presents the local misorientation between different grains. Then, Fig. 8(c) displays the misorientation between different grains within the composites. It is found that the proportion of LAGBs is greater, which can effectively reduce the resistance to dislocation movement and promote the traversal of dislocations between adjacent grains, thus improving the toughness of the composites [12]. Figure 8(d) gives the misorientation between different grains, where LAGBs account for 68.85%. Finally, Fig. 8(e) shows the specific orientations of different grains inside the composites. Since there is no obvious preferential orientation at this point, it can be assumed that HPT promotes the microstructure homogeneity of the composites [7]. At the same time, the grains achieved significant refinement after HPT, which proved that HPT can promote the improvement of mechanical properties

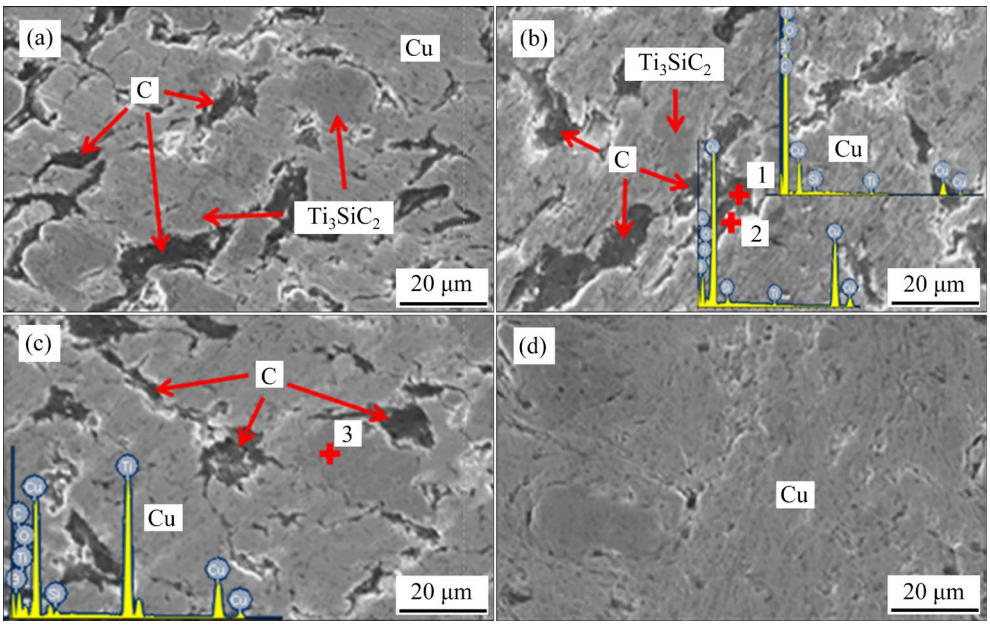

Fig. 7 SEM images of Cu/Ti_3SiC_2/C/MWCNTs nanocomposites with 1 wt.% MWCNTs at different HPT turns: (a) N=0; (b) N=0.5; (c) N=2; (d) N=5

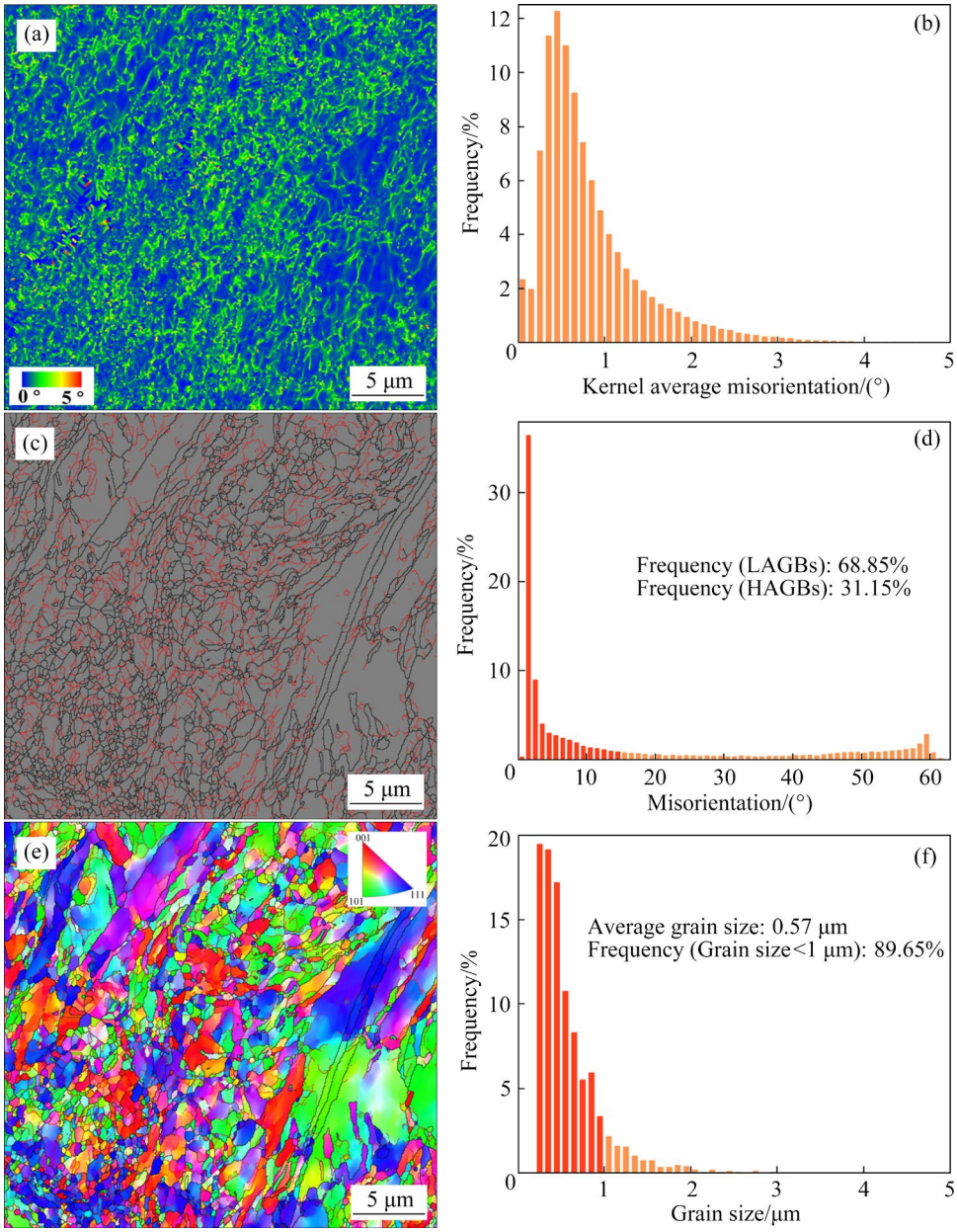

Fig. 8 EBSD results of Cu/Ti_3SiC_2/C/MWCNTs nanocomposites with 1 wt.% MWCNTs after HPT (N=5): (a) Kernel average misorientation (KAM) figure; (b) Histogram of local misorientation; (c) Grain boundary (GB) figure; (d) Histogram of grain boundary misorientation; (e) Inverse pole figure (IPF); (f) Histogram of grain size

through refinement strengthening [36]. Meanwhile, defects such as vacancies near GBs are also able to enhance electrical properties [46]. Figure 8(f) shows the size of different grains, and the average grain size is 0.57 μm. At this point, plenty of nano-grains exist, and the number of nano-grains accounts for 89.65%.

However, a small number of regions with larger grains were still found in the composites after HPT, i.e., there may still be slight size differences between grains in different regions. The reason is that the shear strain introduced by HPT is able to induce dynamic recrystallization of the composites, producing a gradient microstructure with a continuous arrangement of large and small grains [42]. Initially, as the shear strain gradually increases, the number of dislocations rises, sub-grains are produced in larger grains, and smaller grains are deformed along the shear direction. With further increase in shear strain, lamellar structures with coarse and ultra-fine grains appear.

Figure 9 shows TEM results of the composites, including morphologies, selected area electron diffraction (SAED) patterns, and corresponding

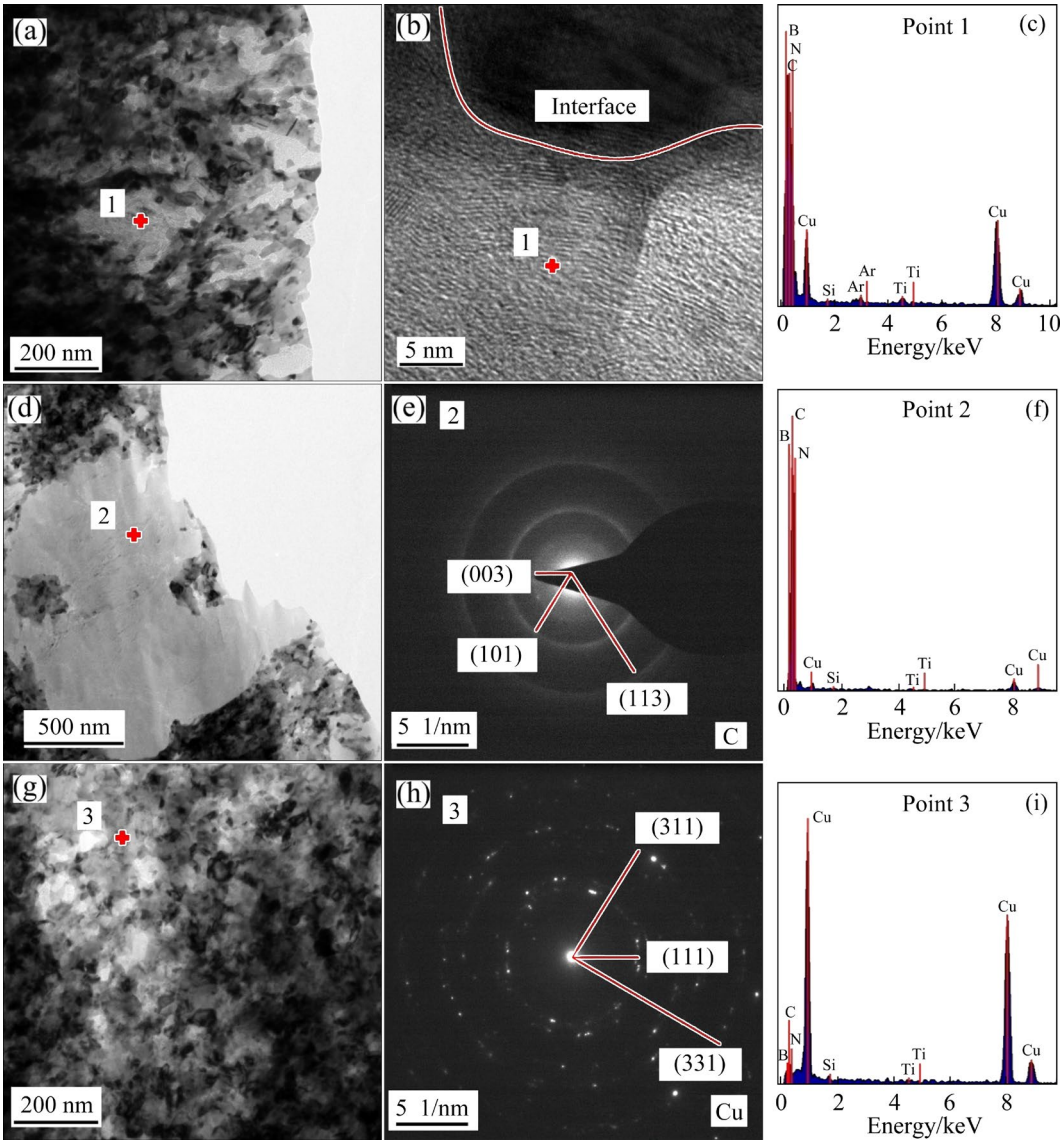

Fig. 9 TEM images of Cu/Ti_3SiC_2/C/MWCNTs nanocomposites with 1 wt.% MWCNTs after HPT (N=5): (a, b, d, g) Morphologies; (e, h) SAED patterns; (c, f, i) EDS results

EDS results. From Figs. 9(a, g), it can be seen that the microstructure of the composites becomes uniform and fine after HPT, and the reinforcing phases are well-dispersed in Cu matrix. At the same time, different grains are tightly bonded to each other, and no defects such as porosity are observed. In the SAED pattern shown in Fig. 9(h), the diffraction spots are disordered and irregular, indicating the superposition of diffraction spots from polycrystals. Meanwhile, the diffraction rings can also be observed in this figure, which is due to the grain refinement of the composites after HPT, and it is also a typical polycrystalline diffraction pattern. Combined with high-resolution images of Point 1 and EDS results (Figs. 9(a−c)), the phase is suggested to be Ti_3SiC_2. Figure 9(b) shows the interfaces between Ti_3SiC_2 and Cu matrix, the interfacial region is blurred and there is a transition layer, which indicates that the interfaces are well bonded. Further analysis shows that the interfacial bonding between Ti_3SiC_2 and Cu matrix is metallurgical, due to the chemical reactions of Ti_3SiC_2 itself at high temperatures, which is favorable to enhancing the performance of the composites by improving the interfacial bonding [8,9,11,12,36]. The interfaces between the translucent phase and Cu matrix shown in Fig. 9(d) are also in close contact, and based on the corresponding SAED pattern and EDS results, it is assumed to be mainly carbon-containing phases,

which can be determined to be graphite. Due to the low bonding strength between graphite flake layers, the shear strain introduced by HPT leads to a reduction in their thickness. Thus, they appear translucent under the microscope [1]. At this point, there are clear interfaces between graphite and Cu matrix, and no diffusion layer is observed, indicating that the bonding type now is mainly mechanical bonding [8,9,11,12,36]. Although the mechanical bonding is usually considered weaker than metallurgical bonding, the absence of pores at the interfaces also indicates that HPT used in this work can obtain tightly bound interfaces, thus effectively improving the mechanical properties of the composites.

3.3 Strengthening mechanisms

Since HPT is a treatment that imposes large plastic deformation on the composites through shear strain, combined with the results of microstructure and properties, the main role of HPT in this work as follows: On the one hand, macroscopically, HPT is a process of gradual densification of the composites, i.e., the change of Cu matrix from loose to close contact. Under severe shear strain, Cu matrix undergoes plastic deformation, and the pores originally existing in the microstructure are squeezed and filled, gradually becoming smaller or even disappearing [8]. This is manifested as an increase in relative density, which further leads to an increase in microhardness and electrical conductivity. On the other hand, microscopically, HPT is a process of refining grains and improving interfacial bonding. Under the synergetic effects of circumferential shear strain and axial pressure, strain accumulates inside the microstructure of the composites, and more dislocations are generated inside the crystal, accompanied by certain slip and twinning [11,12]. At the same time, the grains have certain elasticity, so they also undergo certain deformation which leads to slight movement, and results in refined reinforcing phases under external forces along with the filling of pores. In short, it appears that with increasing HPT turns, the improved microstructure homogeneity, grain refinement, and interfaces blurring are the results.

Figure 10 shows the microstructure evolution of the composites during HPT. To begin with, there are a small number of dislocations in grains of the composites before the sample is subjected to HPT. Next, during the first stage of HPT, the grains are applied to shear strain, dislocations proliferate rapidly and slip, and plastic deformation occurs. As the pressure and shear strain at the edge of the samples are stronger, the deformation is also greater than that of central, resulting in a microstructure with higher dislocation density. Then, as HPT turn increases, the strain accumulated inside the grains keeps increasing. The continuous increase of strain leads to more dislocations inside the crystal and makes dislocation slip, resulting in dislocation plugging. When the dislocation density reaches a certain level, the matrix is already in a high-energy unstable state, and a dynamic recovery process occurs to form LAGBs and then sub-grains. When the misorientation of the surrounding sub-grains is large enough, HAGBs are formed [42]. Finally, when the HPT turn is high enough, ultra-fine equiaxed grains with uniform microstructure will be obtained. Due to the occurrence of dynamic recovery and recrystallization, there are almost no dislocations inside the grains, and the grain boundaries are smooth and flat [42].

According to Hall−Patch effect, the smaller the grain size of the composites is, the better the mechanical properties are [47]. Combined with Tabor relationship, the microhardness of the composites ($HV_{Composite}$) is calculated as follows [48]:

$$HV_{Composite}=(\sigma_0+Kd^{-0.5})/3 \quad (1)$$

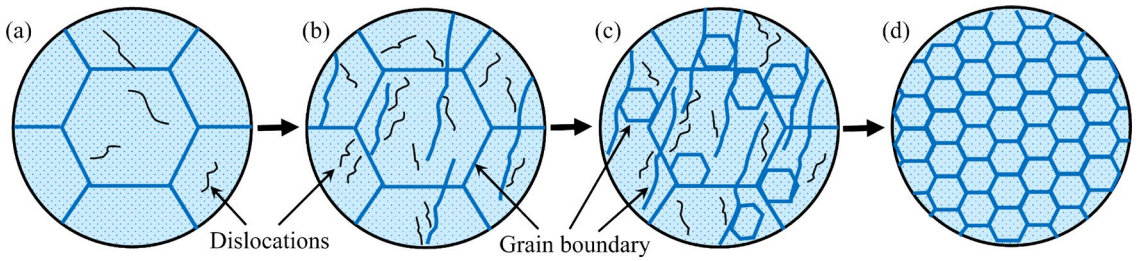

Fig. 10 Schematic diagrams of microstructure evolution during HPT

where σ_0, K, and d represent the intrinsic strength of metal matrix, a constant, and the grain size, respectively. In the absence of significant work hardening, the microhardness of the composites is one-third of its yield strength, and increases with decreasing grain size [47,48]. The higher the HPT shear strain on the grains of the composites, the more pronounced the grain refinement. The synergistic effects of microscopic factors lead to final macroscopic changes, including relative density and microhardness (Figs. 2 and 3).

The improvement of electrical properties in the composites can be explained by the mechanisms related to metal. The rise in defects and pores reduces the free path of electrons, which inevitably leads to a decrease in electrical conductivity [12]. However, the uniform distribution of reinforcing phases and thier favorable interfacial bonding with Cu matrix can promote the formation of the interconnected conductive networks in the composites [32,49]. In current researches, there are problems including interfacial bonding between MWCNTs and Cu matrix. Moreover, as the content of MWCNTs increases, the agglomeration of reinforcing phases will become more obvious, and a certain extent of pores at the interfaces will inevitably arise, which affects the electrical properties of the composites [14].

According to Fuchs size effect theory, the size effect on interfacial resistivity must be considered when the dimension of the composites in any direction is close to the free path of electrons [50]. In this work, $Cu/Ti_3SiC_2/C/MWCNTs$ composites have nano-scale grain size and interfaces when interfacial scattering has an important effect on the electrical properties of the composites. The interfacial resistivity between MWCNTs and Cu matrix ($\rho_{\text{Interface}}$) is calculated as follows [50]:

$$\rho_{\text{Interface}}=\frac{3}{4}\frac{(3\pi^2)^{1/3}\overline{h}}{e^2}(1-p)\frac{V_{\text{MWCNTs}}}{(1-V_{\text{MWCNTs}})d_{\text{i}}}n^{-2/3} \tag{2}$$

where $\overline{h}$, e, p, d_{i}, and n are Planck's constant, electron charge, interfacial scattering coefficient, inner diameter of MWCNTs, and Cu matrix electron concentration, respectively; V_{MWCNTs} is the volume fraction of the second phase. The stronger the interfacial bonding is, the less the scattering of electrons at the interfaces is, the greater the free path of electrons is, the lower the interfacial resistivity is, and the higher the electrical properties of the interfaces are [32,49]. The dispersion of MWCNTs in the composites and the interfacial bonding between MWCNTs and Cu matrix were significantly improved after HPT. At the same time, the relative density of the composites was increased and the number of pores was greatly reduced. All the changes above greatly increased the free path of electrons, as well as the electrical properties of the composites (Fig. 4).

In a word, the addition of a small amount of MWCNTs can improve the mechanical properties of the composites, while excessive amount leads to agglomeration and grain boundary delamination, resulting in the degradation of the properties. As the content of MWCNTs increases, the strength of the composites is improved to a certain level, but it also tends to produce uneven properties between different regions. This is because with increasing MWCNTs content, the porosity between the reinforcing phases and the matrix increases, the stress concentration and the agglomeration of MWCNTs show up near grain boundaries, which prevent the effective transfer of the strengthening effect. The microstructure, mechanical and electrical properties of the composites were all improved after HPT. Therefore, it can be concluded that HPT can be used to obtain balanced mechanical and electrical properties in copper matrix composites.

4 Conclusions

(1) HPT is a purely physical process including microstructure deformation and grain refinement. The higher the HPT turns are, the greater the plastic deformation is, and the better the homogenization and refinement of microstructure are. Moreover, plastic deformation is related to the distance from the center, and the microstructure also changes in a gradient from the center to edge.

(2) The mechanical properties of the composites were significantly improved and distributed in a gradient after HPT. The maximum microhardness values of central and edge from the composites with 1 wt.% MWCNTs reached HV 130.0 and HV 363.5, which were 43.9% and 39.5% higher than those of the original samples, respectively.

(3) The electrical conductivity of the composites was improved as HPT turns increased.

The electrical conductivity of the composites (1 wt.% MWCNTs) with HPT turn N=5 reached 3.42×10^7 S/m, which was 78.1% higher compared to that of raw samples. On the one hand, the porosity was reduced because of increased relative density. On the other hand, the scattering of carriers was decreased due to improved interfacial bonding.

CRediT authorship contribution statement

Zi-xuan WU: Data curation, Writing − Original draft; **Pei-fan ZHANG:** Formal analysis, Validation; **Xiao-song JIANG:** Conceptualization, Funding acquisition, Project administration; Writing − Review & editing; **Hong-liang SUN:** Investigation, Supervision; **Yan-jun LI:** Conceptualization, Funding acquisition; Project administration; Writing − Review & editing; **PÅl CHRISTIAN:** Investigation, Supervision; **Liu YANG:** Methodology, Visualization.

Declaration of competing interest

The authors declare that they have no known competing financial interests or personal relationships that could have appeared to influence the work reported in this paper.

Acknowledgments

This work was supported by Key Laboratory of Infrared Imaging Materials and Detectors, Shanghai Institute of Technical Physics, Chinese Academy of Sciences (No. IIMDKFJJ-21-10), and China Postdoctoral Science Foundation (No. 2018T110993).

References

[1] ZHAO Qi, GAN Xue-ping, ZHOU Ke-chao. Enhanced properties of carbon nanotube-graphite hybrid-reinforced Cu matrix composites via optimization of the preparation technology and interface structure [J]. Powder Technology, 2019, 355: 408−416.

[2] SAMAL C P, PARIHAR J S, CHAIRA D. The effect of milling and sintering techniques on mechanical properties of Cu–graphite metal matrix composite prepared by powder metallurgy route [J]. Journal of Alloys and Compounds, 2013, 569: 95−101.

[3] JIANG Xiao-song, LIU Wan-xia, LI Jing-rui, SHAO Zhen-yi, ZHU De-gui. Microstructures and mechanical properties of $Cu/Ti_3SiC_2/C$/MWCNTs composites prepared by vacuum hot-pressing sintering [J]. Journal of Alloys and Compounds, 2015, 618: 700−706.

[4] JIANG Xiao-song, LIU Wan-xia, LI Yan-jun, SHAO Zhen-yi, LUO Zhi-ping, ZHU De-gui, ZHU Min-hao. Microstructures and mechanical properties of $Cu/Ti_3SiC_2/C$/graphene nanocomposites prepared by vacuum hot-pressing sintering and hot isostatic pressing [J]. Composites (Part B): Engineering, 2018, 141: 203−213.

[5] JIANG Xiao-song, SONG Ting-feng, SHAO Zhen-yi, LIU Wan-xia, ZHU De-gui, ZHU Min-hao. Synergetic effect of graphene and MWCNTs on microstructure and mechanical properties of $Cu/Ti_3SiC_2/C$ nanocomposites [J]. Nanoscale Research Letters, 2017, 12(1): 607.

[6] WU Zi-xuan, JIANG Xiao-song, LI Yan-jun, CHRISTIAN P, SUN Hong-liang, ZHANG Ya-li, FANG Yong-jian, SHU Rui. Microstructures and properties of graphene nanoplatelets reinforced $Cu/Ti_3SiC_2/C$ nanocomposites with efficient dispersion and strengthening achieved by high- pressure torsion [J]. Materials Characterization, 2022, 193: 112308.

[7] ZHANG Xiang, SHI Chun-sheng, LIU En-zuo, HE Fang, MA Li-ying, LI Qun-ying, LI Jia-jun, ZHAO Nai-qin, HE Chun-nian. In-situ space-confined synthesis of well-dispersed three-dimensional graphene/carbon nanotube hybrid reinforced copper nanocomposites with balanced strength and ductility [J]. Composites (Part A): Applied Science and Manufacturing, 2017, 103: 178−187.

[8] JENEI P, GUBICZA J, YOON E Y, KIM H S, LÁBÁR J L. High temperature thermal stability of pure copper and copper−carbon nanotube composites consolidated by high pressure torsion [J]. Composites (Part A): Applied Science and Manufacturing, 2013, 51: 71−79.

[9] JENEI P, YOON E Y, GUBICZA J, KIM H S, LÁBÁR J L, UNGÁR T. Microstructure and hardness of copper–carbon nanotube composites consolidated by high pressure torsion [J]. Materials Science and Engineering A, 2011, 528(13/14): 4690−4695.

[10] AZARNIYA A, AZARNIYA A, SOVIZI S, HOSSEINI H R M, VAROL T, KAWASAKI A, RAMAKRISHNA S. Physicomechanical properties of spark plasma sintered carbon nanotube-reinforced metal matrix nanocomposites [J]. Progress in Materials Science, 2017, 90: 276−324.

[11] AKBARPOUR M R, FARVIZI M, LEE D J, REZAEI H, KIM H S. Effect of high-pressure torsion on the micro-structure and strengthening mechanisms of hot-consolidated Cu-CNT nanocomposite [J]. Materials Science and Engineering A, 2015, 638: 289−295.

[12] AKBARPOUR M R, MOUSA MIRABAD H, ALIPOUR S, KIM H S. Enhanced tensile properties and electrical conductivity of Cu-CNT nanocomposites processed via the combination of flake powder metallurgy and high pressure torsion methods [J]. Materials Science and Engineering A, 2020, 773: 138888.

[13] DAOUSH W M, LIM B K, MO C B, NAM D H, HONG S H. Electrical and mechanical properties of carbon nanotube reinforced copper nanocomposites fabricated by electroless deposition process [J]. Materials Science and Engineering A, 2009, 513/514: 247−253.

[14] MILOWSKA K Z, BURDA M, WOLANICKA L, BRISTOWE P D, KOZIOL K K K. Carbon nanotube functionalization as a route to enhancing the electrical and mechanical properties of Cu-CNT composites [J]. Nanoscale, 2018, 11(1): 145−157.

[15] WU Zi-xuan, JIANG Xiao-song, SUN Hong-liang, SHAO Zhen-yi, SHU Rui, ZHANG Ya-li, FANG Yong-jian. Nano/micro-scale numerical simulation and microscopic analysis

on metal/oxide interfaces: A review [J]. Composites (Part A): Applied Science and Manufacturing, 2022, 163: 107184.

[16] YANG Liu, JIANG Xiao-song, SUN Hong-liang, SHAO Zhen-yi, FANG Yong-jian, SHU Rui. Effects of alloying, heat treatment and nanoreinforcement on mechanical properties and damping performances of Cu−Al-based alloys: A review [J]. Nanotechnology Reviews, 2021, 10(1): 1560−1591.

[17] YANG Liu, JIANG Xiao-song, SUN Hong-liang, ZHANG Ya-li, FANG Yong-jian, SHU Rui. Microstructure and properties of Cu−Al−Ni−Mn−Y alloy with precipitation and effective strengthening by aging treatment [J]. Journal of Alloys and Compounds, 2023, 938: 168658.

[18] YANG Liu, JIANG Xiao-song, SUN Hong-liang, SHAO Zhen-yi, FANG Yong-jian, SHU Rui. Effect of Y on microstructure, damping properties and mechanical properties of Cu−Al−Ni−Mn alloy [J]. Materials Letters, 2022, 308: 131170.

[19] SONG J L, CHEN W G, DONG L L, WANG J J, DENG N. An electroless plating and planetary ball milling process for mechanical properties enhancement of bulk CNTs/Cu composites [J]. Journal of Alloys and Compounds, 2017, 720: 54−62.

[20] SHAO Zhen-yi, PAN Heng-kang, SHU Rui, JIANG Xiao-song, ZHU Min-hao. Microstructures and interfacial interactions of Al_2O_3 whiskers and graphene nano-platelets co-reinforced copper matrix composites [J]. Transactions of Nonferrous Metals Society of China, 2022, 32(9): 2935−2947.

[21] DU Qing-lin, LI Chang, CUI Xiao-hui, KONG C, YU Hai-liang. Fabrication of ultrafine-grained AA1060 sheets via accumulative roll bonding with subsequent cryorolling [J]. Transactions of Nonferrous Metals Society of China, 2021, 31(11): 3370−3379.

[22] HE Tian-bing, HE Xiao-lei, TANG Peng-jun, CHU De-sheng, WANG Xing-yuan, LI Pei-yong. The use of cryogenic milling to prepare high performance Al2009 matrix composites with dispersive carbon nanotubes [J]. Materials & Design, 2017, 114: 373−382.

[23] CHA S I, KIM K T, ARSHAD S N, MO C B, HONG S H. Extraordinary strengthening effect of carbon nanotubes in metal-matrix nanocomposites processed by molecular-level mixing [J]. Advanced Materials, 2005, 17(11): 1377−1381.

[24] VALIEV R Z, IVANISENKO Y V, RAUCH E F, BAUDELET B. Structure and deformation behaviour of Armco iron subjected to severe plastic deformation [J]. Acta Materialia, 1996, 44(12): 4705−4712.

[25] HUANG Zi-xin, ZHENG Zhong, ZHAO Shan, DONG Shi-jie, LUO Ping, CHEN Lie. Copper matrix composites reinforced by aligned carbon nanotubes: Mechanical and tribological properties [J]. Materials & Design, 2017, 133: 570−578.

[26] ZHAO Shan, ZHENG Zhong, HUANG Zi-xin, DONG Shi-jie, LUO Ping, ZHANG Zhuang, WANG Yao-wei. Cu matrix composites reinforced with aligned carbon nanotubes: Mechanical, electrical and thermal properties [J]. Materials Science and Engineering A, 2016, 675: 82−91.

[27] XIONG Ni, BAO Rui, YI Jian-hong, TAO Jing-mei, LIU Yi-chun, FANG Dong. Interface evolution and its influence on mechanical properties of CNTs/Cu-Ti composite [J]. Materials Science and Engineering A, 2019, 755: 75−84.

[28] LIU Liang, BAO Rui, YI Jian-hong, LI Cai-ju, TAO Jing-mei, LIU Yi-chun, TAN Song-lin, YOU Xin. Well-dispersion of CNTs and enhanced mechanical properties in CNTs/Cu−Ti composites fabricated by molecular level mixing [J]. Journal of Alloys and Compounds, 2017, 726: 81−87.

[29] CHU Ke, JIA Cheng-chang, JIANG Li-kun, LI Wen-sheng. Improvement of interface and mechanical properties in carbon nanotube reinforced Cu−Cr matrix composites [J]. Materials & Design, 2013, 45: 407−411.

[30] FU Shao-li, CHEN Xiao-hong, LIU Ping. Preparation of CNTs/Cu composites with good electrical conductivity and excellent mechanical properties [J]. Materials Science and Engineering A, 2020, 771: 138656.

[31] WANG Hu, ZHANG Zhao-hui, ZHANG Hong-mei, HU Zheng-yang, LI Sheng-lin, CHENG Xing-wang. Novel synthesizing and characterization of copper matrix composites reinforced with carbon nanotubes [J]. Materials Science and Engineering A, 2017, 696: 80−89.

[32] WEI Xia, TAO Jing-mei, HU Yong, LIU Yi-chun, BAO Rui, LI Feng-xian, FANG Dong, LI Cai-ju, YI Jian-hong. Enhancement of mechanical properties and conductivity in carbon nanotubes (CNTs)/Cu matrix composite by surface and intratube decoration of CNTs [J]. Materials Science and Engineering A, 2021, 816: 141248.

[33] WANG Zi-yang, CAI Xiao-lan, YANG Chang-jiang, ZHOU Lei. Improving strength and high electrical conductivity of multi-walled carbon nanotubes/copper composites fabricated by electrodeposition and powder metallurgy [J]. Journal of Alloys and Compounds, 2018, 735: 905−913.

[34] WANG Zi-yang, CAI Xiao-lan, YANG Chang-jiang, ZHOU Lei, HU Cui. An electrodeposition approach to obtaining carbon nanotubes embedded copper powders for the synthesis of copper matrix composites [J]. Journal of Alloys and Compounds, 2018, 735: 1357−1362.

[35] AN Z L, TODA M, ONO T. Comparative investigation into surface charged multi-walled carbon nanotubes reinforced Cu nanocomposites for interconnect applications [J]. Composites (Part B): Engineering, 2016, 95: 137−143.

[36] LI Hong-qi, MISRA A, ZHU Yun-tian, HORITA Z, KOCH C C, HOLESINGER T G. Processing and characterization of nanostructured Cu−carbon nanotube composites [J]. Materials Science and Engineering A, 2009, 523(1/2): 60−64.

[37] CHU Ke, WU Qing-ying, JIA Cheng-chang, LIANG Xue-bing, NIE Jun-hui, TIAN Wen-huai, GAI Guo-sheng, GUO Hong. Fabrication and effective thermal conductivity of multi-walled carbon nanotubes reinforced Cu matrix composites for heat sink applications [J]. Composites Science and Technology, 2010, 70(2): 298−304.

[38] SABIROV I, KOLEDNIK O, VALIEV R Z, PIPPAN R. Equal channel angular pressing of metal matrix composites: Effect on particle distribution and fracture toughness [J]. Acta Materialia, 2005, 53(18): 4919−4930.

[39] YAO G C, MEI Q S, LI J Y, LI C L, MA Y, CHEN F, LIU M. Cu/C composites with a good combination of hardness and electrical conductivity fabricated from Cu and graphite by accumulative roll-bonding [J]. Materials & Design, 2016,

110: 124−129.
[40] CHEN F, MEI Q S, LI J Y, LI C L, WAN L, ZHANG G D, MEI X M, CHEN Z H, XU T, WANG Y C. Fabrication of graphene/copper nanocomposites via in-situ delamination of graphite in copper by accumulative roll-compositing [J]. Composites (Part B): Engineering, 2021, 216: 108850.
[41] ZHANG Z W, LIU Z Y, XIAO B L, NI D R, MA Z Y. High efficiency dispersal and strengthening of graphene reinforced aluminum alloy composites fabricated by powder metallurgy combined with friction stir processing [J]. Carbon, 2018, 135: 215−223.
[42] ZHILYAEV A P, LANGDON T G. Using high-pressure torsion for metal processing: Fundamentals and applications [J]. Progress in Materials Science, 2008, 53(6): 893−979.
[43] ROGACHEV S O, NIKULIN S A, KHATKEVICH V M, SUNDEEV R V, KOZLOV D A. High-pressure torsion deformation process of bronze/niobium composite [J]. Transactions of Nonferrous Metals Society of China, 2019, 29(8): 1689−1695.
[44] DENG Hui, YI Jian-hong, XIA Chao, YI Yi. Mechanical properties and microstructure characterization of well-dispersed carbon nanotubes reinforced copper matrix composites [J]. Journal of Alloys and Compounds, 2017, 727: 260−268.
[45] DUAN Bo-hua, ZHOU Yu, WANG De-zhi, ZHAO Ying-rui. Effect of CNTs content on the microstructures and properties of CNTs/Cu composite by microwave sintering [J]. Journal of Alloys and Compounds, 2019, 771: 498−504.
[46] XU C L, WEI B Q, MA R Z, LIANG J, MA X K, WU D H. Fabrication of aluminum–carbon nanotube composites and their electrical properties [J]. Carbon, 1999, 37: 855−858.
[47] SHU Rui, JIANG Xiao-song, SUN Hong-liang, SHAO Zhen-yi, SONG Ting-feng, LUO Zhi-ping. Recent researches of the bio-inspired nano-carbon reinforced metal matrix composites [J]. Composites Part A: Applied Science and Manufacturing, 2020, 131: 105816.
[48] BRADBURY C R, GOMON J, KOLLO L, KWON H, LEPAROUX M. Hardness of multi wall carbon nanotubes reinforced aluminium matrix composites [J]. Journal of Alloys and Compounds, 2014, 585: 362−367.
[49] YANG Ping, YOU Xin, YI Jian-hong, FANG Dong, BAO Rui, SHEN Tao, LIU Yi-chun, TAO Jing-mei, LI Cai-ju. Influence of dispersion state of carbon nanotubes on electrical conductivity of copper matrix composites [J]. Journal of Alloys and Compounds, 2018, 752: 376−380.
[50] TIAN L, ANDERSON I, RIEDEMANN T, RUSSELL A. Modeling the electrical resistivity of deformation processed metal–metal composites [J]. Acta Materialia, 2014, 77: 151−161.

高压扭转提高多壁碳纳米管增强 $Cu/Ti_3SiC_2/C$ 纳米复合材料的力学和电学性能

武子轩[1,2,3]，张沛帆[4]，蒋小松[1,2]，孙红亮[1,2]，李彦军[5]，PÅL CHRISTIAN[5]，杨 刘[6]

1. 西南交通大学 材料先进技术教育部重点实验室，成都 610031；
2. 西南交通大学 材料科学与工程学院，成都 610031；
3. School of Engineering and Materials Science, Queen Mary University of London, London E1 4NS, United Kingdom;
4. 海军航空大学 教研保障中心，烟台 264001；
5. Department of Materials Science and Engineering, Norwegian University of Science and Technology, Trondheim 7491, Norway;
6. Institute for Applied Materials, Karlsruhe Institute of Technology, Karlsruhe 76131, Germany

摘 要：为了获得综合的力学和电学性能，通过高压扭转对多壁碳纳米管增强 $Cu/Ti_3SiC/C$ 纳米复合材料进行进一步加工。含 1%(质量分数)多壁碳纳米管复合材料中心和边缘的最大显微硬度值分别达到 HV 130.0 和 HV 363.5，相比原始样品分别提高了 43.9%和 39.5%。其电导率的最大值达到 3.42×10^7 S/m，相比原始样品提高了 78.1%。力学和电学性能的协同提高归因于均匀化和细化的显微组织，以及改善的界面结合和降低的孔隙率。增强机理包括与力学性能相关的弥散和细晶强化，以及与电学性能相关的电子散射的减少。

关键词：$Cu/Ti_3SiC/C$ 纳米复合材料；多壁碳纳米管；高压扭转；显微组织；显微硬度；电导率

(Edited by Wei-ping CHEN)